Optik - International Journal for Light and Electron Optics 188 (2019) 225–232

Contents lists available at ScienceDirect

Optik

journal homepage: www.elsevier.com/locate/ijleo

Original research article

Performance analysis of weather research and forecasting model for simulating near-surface optical turbulence over land

Chun Qing, Xiaoqing Wu, Xuebin Li, Wenyue Zhu*

Key Laboratory of Atmospheric Optics, Anhui Institute of Optics and Fine Mechanics, Chinese Academy of Sciences, Hefei 230031, China

ARTICLE INFO

Keywords:
Atmospheric optics
Laser beam transmission
Mesoscale model
Optical turbulence

ABSTRACT

Accurate knowledge of the optical turbulence (C_n^2) in the atmospheric surface layer is of great significance for the applications of various ground-based optical systems (e.g., astronomical observation, laser communication and target detection), however, many methods using instruments to measure C_n^2 are limited spatially and temporally and they are more difficult and expensive in severe environments, which makes estimations a less expensive and convenient alternative. This study introduces a method where the products of Weather Research and Forecasting (WRF) model coupled with Monin–Obukhov similarity (MOS) theory is used to estimate the value of C_n^2 in the surface layer, and the performance of this method is evaluated against the corresponding C_n^2 dataset from the *in-situ* micro-thermometer during a campaign over south-west China. The variance between the estimated C_n^2 and measured C_n^2 is found to be comparable to the observed variance of the temporal due to temporal and spatial variations of the atmospheric turbulence. Evaluation against direct observations shows that this approach can well estimate C_n^2 time series with some error in some time periods, and both the estimated C_n^2 and the measured C_n^2 are more consistent in trend and magnitude in general. Given these validated results, this method has the potential to be a useful tool in a wide range of ground-based optical applications.

1. Introduction

Atmospheric turbulence intensity is usually characterized by the refractive index structure constant (C_n^2, $m^{-2/3}$), and various parameters with C_n^2 as the integral parameter such as the seeing (ε), the isoplanatic angle (θ_0) and the wavefront coherence time (τ_0) are important for studying the effect of laser transmission in the atmosphere [1–3].

Various instruments such as Scintillometer [4], Interferometers [5], Differential Image Motion Monitor (DIMM) [6], Microthermometry (Balloon) [7], Scintillation Detection and Ranging (SCIDAR) [8], Multi Aperture Scintillation Sensor (MASS) [9] have been used to measure these atmospheric turbulence parameters. These instruments are not easy to operate and are quite expensive, thus, it makes the instruments difficult to perform with a large-scale, long-term, systematic observation, and also in strong winds and freezing conditions they seem too fragile to obtain reliable results. Therefore, there is a need for a robust method for estimating C_n^2 based on readily routine meteorological parameters (e.g., temperature, relative humidity, pressure, wind speed, etc.).

Monin–Obukhov similarity (MOS) theory provides an important theoretical basis to obtain C_n^2 from routine meteorological parameters [10–15]. Over the years, Masciadri and Lascaux have used Mesoscale Non-hydrostatic (Meso-Nh) model to obtain C_n^2 profile above the sites of interest for astronomy (e.g., Roque de Los Muchachos Observatory; European Southern Observatory)

* Corresponding author.
E-mail address: zhuwenyue@aiofm.ac.cn (W. Zhu).

https://doi.org/10.1016/j.ijleo.2019.05.023
Received 7 March 2019; Accepted 6 May 2019

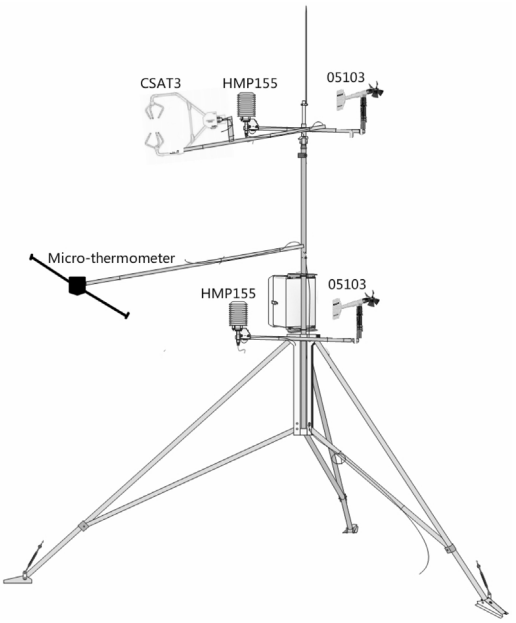

Fig. 1. The *in-situ* measurement system.

[16–21]. However, using Weather Research and Forecasting (WRF) model and Monin–Obukhov similarity (MOS) theory to estimate C_n^2 in the surface layer is seldom reported. On account of the various ground based optical application requirements, the purpose of this paper is to present a significative result of estimated C_n^2 in the surface layer over land, and this method can be used for gap filling in case of failures of the instruments.

The remainder of this paper is organized as follows. The detailed description of *in-situ* measurement and the configuration of modeling are given in Section 2. The methodologies of estimating C_n^2 is introduced in Section 3. The estimation C_n^2 results and the related statistical analysis are shown in Section 4. Finally, conclusions and discussion are given in Section 5.

2. Data and methodologies

2.1. The description of observational site and environment

The measurement place is located in Chengdu area (south-west China) in which belongs to a subtropical wet monsoon climate. Because of its topography and other special geographical and environmental factors, it also has a prominent vertical climate. The *in-situ* measurement system includes a data logger (CR5000, details specifications are given in the manufacturer https://campbell.secure.force.com/campbellsite), ultrasonic anemometer (CSAT3), micro-thermometer, temperature and relative humidity probe (HMP155), wind speed & direction sensors (05103), CS106 barometer, 485 communication module, power module and a 3-m tower, which are shown in Fig. 1.

HMP155 sensor and 05103 sensor are installed on the first floor, approximately 1 m above the ground. CSAT3 ultrasonic anemometers and micro-thermometer are installed on the second floor approximately 3 m above the ground. The underlying surface of observational site is low shrubbery and grassland, but there is a house about 60 m high and 500 m away from the measurement site.

Table 1
Main technical specification of the *in-situ* measurement system. Note that temperature, relative humidity, wind speed, wind direction and pressure are abbreviated as T, RH, WS, WD and P in the table.

Instrument	Parameter	Range	Accuracy
Micro-thermometer	C_n^2	$10^{-18}\sim10^{-12}$ m$^{-2/3}$	
CSAT3	WS	u_x: ± 30 m·s^{-1} u_y: ± 30 m·s^{-1} u_z: ± 8 m·s^{-1}	$u_x \leqslant$ ± 4 cm·s^{-1} $u_y \leqslant$ ± 4 cm·s^{-1} $u_z \leqslant$ ± 2 cm·s^{-1}
HMP155 sensor	T	−40 ~ +60 °C	⩽ ± 0.5°C
	RH	0 ~ 100%	± 1%
05103 sensor	WS	0 ~ 100 m·s^{-1}	0.5 m·s^{-1}
	WD	0 ~ 360°	3°
CS106 barometer	P	500 ~ 1100 hPa	± 0.3 hPa @20°C

The main technical indicators of the *in-situ* measurement system are shown in Table 1.

2.2. C_n^2 data from the micro-thermometer

For visible and near-infrared wavelengths light, C_n^2 is mainly caused by temperature fluctuation. In this study, C_n^2 values deduced from the micro-thermometer are used for comparison, and they are measured by a pair of horizontally micro-temperature probes. Temperature structure function $D_T(r)$ is one of statistics describing temperature disturbance at two points separated by distance r [22], and is given by

$$D_T(r) = \langle [T(\vec{x}) - T(\vec{x} + \vec{r})]^2 \rangle, \quad l_0 \ll r \ll L_0, \tag{1}$$

where T is air temperature (K), $\vec{x}$ and $\vec{r}$ denote the position vector, r is the magnitude of $\vec{r}$, $\langle . .. \rangle$ represents ensemble average, l_0 and L_0 are the inner and outer scales of atmospheric turbulence. When r is between l_0 and L_0, this function appears as a power law in $r^{2/3}$. These scales can be seen as the minimum and maximum sizes of turbulent eddies. In the inertia range $[l_0, L_0]$, defines the structure constant of temperature (C_T^2) as below

$$D_T(r) = C_T^2 r^{2/3}, \quad l_0 \ll r \ll L_0. \tag{2}$$

The relationship between C_n^2 and C_T^2 is expressed by [23] and using the Gladstone's law that relates the refractive index to temperature structure constant, C_n^2 is expressed as

$$C_n^2 = \left(79 \times 10^{-6} \frac{P}{T^2}\right)^2 C_T^2, \tag{3}$$

where P is air pressure (hPa).

The two probes are legs of a Wheatstone bridge, and the resistance of probe is nearly proportional to temperature, thus, the temperature change can be transformed into the resistance change to obtain the voltage change. The micro-thermometer system provides C_T^2 data by measuring mean square temperature fluctuations from Eq. (1) and thus C_n^2 value can be acquired from Eqs. (2)–(3). In our case, a 10 μm diameter platinum wire has a standard deviation of minimum temperature fluctuation is less than 0.002 K [24].

In order to verify the performance of this method, 6 days of available C_n^2 observations data measured by micro-thermometer are used to as a comparison. The average routine meteorological parameters and weather conditions during the period of experiment are listed in Table 2.

2.3. Model configuration

WRF model is a mesoscale atmospheric model, which is developed by the National Centers for Environmental Prediction (NCEP) and the National Center for Atmospheric Research (NCAR) of the United States. Detailed control equations, transformations and grid adaptation, see the User's Guide [25]. In this study, the Advance Research WRF (ARW) model is used to conduct simulations.

There are 40 vertical levels and three nested horizontal domains with horizontal resolutions of 9 km, 3 km, and 1 km, respectively, in each simulation. The center grid point (30.57°N, 104.02°E) of the finest nested grid is close to *in-situ* measurement system. The final operational global analysis (FNL) data with $1^\circ \times 1^\circ$ horizontal resolution and 6-h temporal resolution is used to initialize the input to the WRF model, which is downloaded from the web site of NCEP. The outputs are saved as 10 min intervals, and the results from first 24 h are excluded to avoid errors. WRF model relies on a selected physical schemes to output multiple meteorological parameters, see User's Guide to gain a better understanding of mesoscale modeling, and model configurations and main physical scheme options are summarized in Table 3.

3. The methodologies of estimating C_n^2

According to Monin-Obukhov similarity theory, C_n^2 can be defined in terms of the temperature structure parameter (C_T^2), humidity structure parameter (C_q^2) and temperature-humidity structure parameter (C_{Tq}) as follows [34]:

Table 2
Average routine meteorological parameters and weather conditions during the period of experiment. Note that temperature, relative humidity, wind speed and pressure are abbreviated as T, RH, WS and P in the table.

Date	T (°C)	RH (%)	P (hPa)	WS ($m \cdot s^{-1}$)	Weather condition
2014-5-1	19.5	54	956	2.2	Cloudy
2014-5-2	18.0	55	961	1.7	Overcast
2014-5-6	20.0	45	957	2.0	Sunny
2014-5-7	21.5	50	954	2.3	Sunny
2014-5-12	22.5	49	951	2.0	Cloudy
2014-5-13	22.0	52	948	1.9	Cloudy

Table 3
WRF model configurations.

Attribute	Model Configuration
Simulation period	1–13 May 2014
Domain	Nested regional domains
Center longitude and latitude	104.02°E, 30.57°N
Horizontal resolution, grid point numbers	9 km, 90 × 90 (Coarse Grid) 3 km, 75 × 75 (Fine Grid) 1 km, 45 × 45 (Finest Grid)
Vertical resolution	40 layers from 1000-10 hPa
Initialized meteorological data	NCEP-FNL
Microphysics	WSM-5 [26]
Longwave Radiation	RRTM [27]
Shortwave Radiation	Goddard [28]
Surface Layer	Eta similarity [29]
Land Surface	NOAH [30,31]
Planetary boundary layer	MYJ [32,33]

$$C_n^2 = A^2 C_T^2 + 2\mathrm{ABC}_{\mathrm{Tq}} + B^2 C_q^2 \ . \tag{4}$$

At a interest wavelength of 0.55 μm, A = $79.0\times 10^{-6}\frac{P}{T^2}$ and B = -56.4×10^{-6}. The structure constant C_T^2, C_q^2 and C_{Tq} can be expressed as follows:

$$C_T^2 = T_*^2 z^{-2/3} f_T(z/L) \ , \tag{5a}$$

$$C_q^2 = q_*^2 z^{-2/3} f_q(z/L) \ , \tag{5b}$$

$$C_{\mathrm{Tq}} = \gamma_{\mathrm{Tq}} T_* q_* z^{-2/3} f_{\mathrm{Tq}}(z/L) \ , \tag{5c}$$

where z is the height above the surface, L is the Obukhov length. T_* and q_* are the scaling parameters for temperature, specific humidity, respectively. γ_{Tq} is the correlation coefficient. The similarity functions $f_T(z/L)$, $f_q(z/L)$ and $f_{Tq}(z/L)$ are experimentally determined, and the well-known similarity function is given by [10]:

$$f(z/L) = \begin{cases} 4.9(1-7z/L)^{-2/3}, & z/L < 0, \\ 4.9[(1+2.4(z/L)^{2/3}], & z/L > 0. \end{cases} \tag{6}$$

Subsequently, substituting Eq. (5a) into Eq. (4) gives a C_n^2 expression in terms of T_*, q_* and L as below:

$$C_n^2 = z^{-2/3} f(z/L)(\mathrm{A}^2 T_*^2 + 2\mathrm{AB}\gamma_{\mathrm{Tq}} T_* q_* + \mathrm{B}^2 q_*^2). \tag{7}$$

From Monin-Obukhov similarity theory, conditions are assumed to be horizontally homogeneous and stationary, and it is possible to define T_*, q_* and u_* in terms of mean horizontal-vertical velocity covariance ($\bar{\omega u}$), mean vertical velocity-temperature convariance ($\bar{\omega T}$) and mean vertical velocity-water vapour density convariance ($\bar{\omega q}$) [35] as follows:

$$u_*^2 = -\bar{\omega u} \ , \tag{8a}$$

$$u_* T_* = -\bar{\omega T} \ , \tag{8b}$$

$$u_* q_* = -\bar{\omega q} \tag{8c}$$

where u is the horizontal component of turbulent velocity vector, and ω is the vertical component of turbulent velocity vector.

The bulk aerodynamic formulas are simple empirical parameterizations of the surface fluxes in the surface layer in terms of average surface layer variables, which are given by:

$$u_*^2 = C_D \bar{U}^2 \ , \tag{9a}$$

$$\bar{\omega T} = C_H \bar{U}[T_s - T(z)] = C_H \bar{U} \Delta T \ , \tag{9b}$$

$$\bar{\omega q} = C_E \bar{U}[q_s - q(z)] = C_E \bar{U} \Delta q \ , \tag{9c}$$

where $\bar{U}$ is the mean wind speed at height z, and $\Delta T = T_s - T(z)$, $\Delta q = q_s - q(z)$. $T(z)$ and $q(z)$ are mean air temperature, mean specific humidity at height z, respectively. T_s and q_s are the surface temperature, specific humidity, respectively. C_D, C_H and C_E are the drag coefficient, sensible heat flux coefficient and moisture flux coefficient, respectively.

Consequently, substituting Eq. (9a) into Eq. (8a) gives the expression T_*, q_* and u_* as follow:

$$u_*^2 = C_D \bar{U}^2 \ , \tag{10a}$$

$$T_* = -\frac{C_H \bar{U}\Delta T}{u_*}\ , \tag{10b}$$

$$q_* = -\frac{C_E \bar{U}\Delta q}{u_*}\ . \tag{10c}$$

The drag coefficient (C_D), sensible heat flux coefficient (C_H) and moisture flux coefficient (C_E) are all from experiment [36]:

$$C_D = 1.3 \times 10^{-3}\ , \tag{11a}$$

$$C_H = \begin{cases} 0.91 \times 10^{-3}\ , & -20 < \bar{U}\Delta T < 25\ (\mathrm{mKs^{-1}}), \\ 1.46 \times 10^{-3}\ , & \bar{U}\Delta T > 25\ (\mathrm{mKs^{-1}}). \end{cases} \tag{11b}$$

$$C_E = 1.32 \times 10^{-3}. \tag{11c}$$

For the parameterization of Obukhov length L, the expression of L is given by two $\bar{U}\Delta T$ ranges as follow:

$$L^{-1} = \begin{cases} -0.231\left(\dfrac{\Delta T}{\bar{U}^2} + 0.212\dfrac{\Delta q}{\bar{U}^2}\right), & -20 < \bar{U}\Delta T < 25\ (\mathrm{mKsec^{-1}}), \\ -0.371\left(\dfrac{\Delta T}{\bar{U}^2} + 0.132\dfrac{\Delta q}{\bar{U}^2}\right), & \bar{U}\Delta T > 25\ (\mathrm{mKsec^{-1}}). \end{cases} \tag{12}$$

Therefore, the values of $U(z)$, $T(z)$ and $q(z)$, as well as T_s and q_s are exported by WRF model first, then air-surface difference for temperature (ΔT), specific humidity (Δq) and mean wind speed ($\bar{U}$) are calculated. u_*, T_*, q_* and L can be obtained by solving Eqs. (10a)–(12). Finally, it is simple to calculate C_n^2 from Eqs. (6)–(7).

4. Results

Fig. 2 shows the C_n^2 time-series between estimated by WRF model and *in-situ* measured by micro-thermometer in the surface layer. For ease of comparison, the measured values are also superimposed on the figure. It can be seen that both the estimated C_n^2 and that measured by micro-thermometer are more consistent in trend and magnitude in general. The estimated C_n^2 values tend to be underestimated in the nighttime, however, in the strong turbulence are more accurate.

As we all know that Wyngaard proposed a similarity function model to estimate C_n^2 in the atmospheric surface layer [10], and the

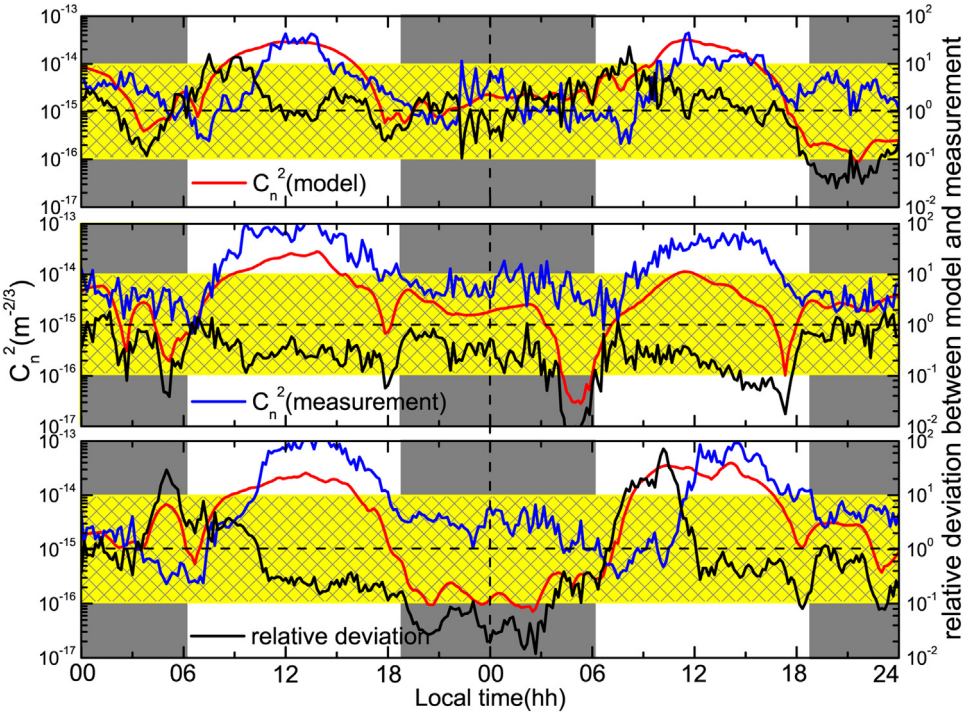

Fig. 2. The time-series of C_n^2 in the surface layer. The red line and blue line represent the estimation and measurement, and the black line represents the relative deviation (right ordinate), respectively. The gray shade indicates the nighttime, and the yellow shaded area denotes the relative deviation in the range [0.1, 10]. Note that local time = UTC + 8h.

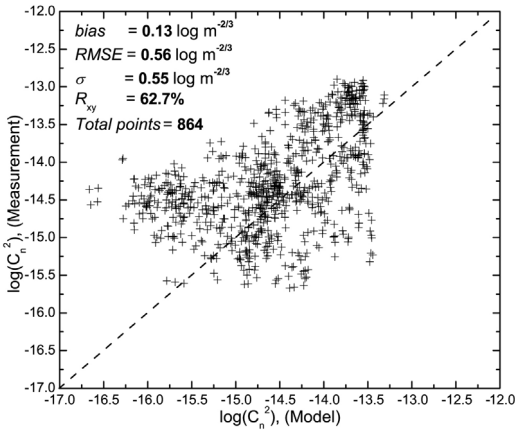

Fig. 3. Scatter diagrams of C_n^2 between estimation and measurement, and each cross point represents an average of 10 min resolution.

performance of this similarity function model is satisfactory well under unstable conditions, but it is not very good under stable conditions. Literature pointed out that this similarity function model only covers a relatively short atmospheric stability range, and thus significantly limits its applicability at night under stable conditions [37]. Therefore, there is a need for constructing a new similarity function model which covers a wide range of atmospheric stabilities conditions in the future work. From Fig. 2, the fluctuations of relative deviation between the estimated C_n^2 and the measured C_n^2 are generally within 10 times, and the relative deviation between the two will be greater at night and the atmosphere is under stable conditions.

Three statistical operators: *bias*, root mean square error (*RMSE*), bias-corrected *RMSE* (σ), and the correlation coefficient (R_{xy}) are used to evaluate the accuracy of estimated C_n^2, which follows the same framework as [21]. For convenience, C_n^2 is plotted on the logarithmic scale. The correlation of the $\log(C_n^2)$ between estimation and measurement is depicted in Fig. 3, one can see that the *bias*, *RMSE* and σ are relatively small, and R_{xy} is relatively large, showing the estimation is coherent with the measurement well.

In addition, a 3×3 contingency tables are used to study the relationship between model values and measured values, referring to the paper for details [21]. A contingency table allows for analysis of the relationship between two or more categorical variables, which is a table with $n \times n$ entries that displays the distribution of model and measurement in terms of frequencies or relative frequencies. An example of a 3×3 contingency table is shown in Table 4, and there are two cases in which a "hit" representing the estimated value is correct, yet a "miss" representing the estimated value is incorrect.

Using a, b, c, d, e, f, g, h, i and N ($N = a + b + c + d + e + f + g + h + i$), some probabilities parameters can be calculated which are used to investigate how well (or bad) this method performs for a particular parameter. Some evaluation parameters we will use in the following paper from the generic 3×3 contingency table of Table 4: percent of correct detections (*PC*, in %), probability of detection (*POD*, in %) and extremely bad detection (*EBD*, in %) are listed. In a random estimation case, all *POD* are equal to 33%, $PC = 33\%$, $EBD = 22.2\%$, and the estimation will be useful if these values (*PC*, *POD*, *EBD*) perform better than those random cases. These parameters are a good reference to evaluate the performances of this approach, and we will write POD_i instead of *POD* (*event i*) with the i event considered.

$$\mathrm{PC} = \frac{a+e+i}{N} \times 100\ ,\quad 0\% \leqslant \mathrm{PC} \leqslant 100\%\ , \tag{13a}$$

$$\mathrm{POD(event\ 1)} = \frac{a}{a+d+g} \times 100\ ,\quad 0\% \leqslant \mathrm{POD} \leqslant 100\%\ , \tag{13b}$$

$$\mathrm{POD(event\ 2)} = \frac{e}{b+e+h} \times 100\ ,\quad 0\% \leqslant \mathrm{POD} \leqslant 100\%\ , \tag{13c}$$

$$\mathrm{POD(event\ 3)} = \frac{i}{c+f+i} \times 100\ ,\quad 0\% \leqslant \mathrm{POD} \leqslant 100\%\ , \tag{13d}$$

Table 4
A generic 3×3 contingency table.

		Measurement			
	Intervals	1	2	3	Total
Model	1	a (hit 1)	b	c (miss)	$a+b+c$
	2	d	e (hit 2)	f	$d+e+f$
	3	g (miss)	h	i (hit 3)	$g+h+i$
	Total	$a+d+g$	$b+e+h$	$c+f+i$	N

Table 5
3 × 3 contingency table of $\log(C_n^2)$ ($m^{-2/3}$) for WRF model and micro-thermometer in surface layer, this two thresholds -14.7 and -14.2 are defined with the climatological tertiles. Note that $PC = 50.1\%$, $EBD = 8.1\%$, $POD_1 = 48.1\%$, $POD_2 = 37.5\%$, $POD_3 = 63.7\%$.

		Measurement			
	Intervals	[, -14.7]	[-14.7, -14.2]	[-14.2,]	Total
Model	[, -14.7]	88	169	40	297
	[-14.7, -14.2]	65	127	84	276
	[-14.2,]	30	43	218	291
	Total	183	339	342	864

$$\mathrm{EBD} = \frac{c+g}{N} \times 100\ , \quad 0\% \leqslant \mathrm{EBD} \leqslant 100\%\ . \tag{13e}$$

In Table 5, the *PC* (50.1%) is significatively better than 33%. Moreover, the *EBD* (8.1%) is small which is the sign that this approach seldom produces extremely bad simulation. POD_1 is 48.1%, POD_2 is 37.5% and POD_3 is 63.7%. In all cases, *PC* and $POD_{i=1,2,3}$ are well larger than 33%.

5. Conclusions and discussion

The main result of this paper is that WRF model coupling MOS theory is used to rebuild the time-series of C_n^2 in the surface layer over southwest China, and the results of this study provide an alternative way to obtain C_n^2 when using optoelectronic systems in some scenes that are difficult to measure. Analysis shows that the C_n^2 values between estimation and measurement are more consistent in trend and magnitude in general, however, the estimated C_n^2 values tend to be underestimated in the nighttime. It should be pointed out that the similarity function model (W73, [10]) we use in this study only covers a relatively short atmospheric limited range, therefore, there is a need for constructing a new similarity function model in the future work. Furthermore, MOS theory makes an assumption of horizontal homogeneity, and the sensible heat flux and latent heat flux are really small in the nighttime, thus the sensible heat flux and latent heat flux yielded from WRF model output which may involve more complex error source. To be certain, more validation studies would be carried out in next work.

Acknowledgements

We are indebted to the NCAR and NCEP for granting access to their products. This work is funded by China Postdoctoral Science Foundation (2017M622034, 2018T110632); National Natural Science Foundation of China (41576185).

References

[1] V.I. Tatarskii, The effects of the turbulent atmosphere on wave propagation, (1971).
[2] J.L. Lumley, A.M. Yaglom, A century of turbulence, Flow Turbul. Combus. 66 (2001) 241–286.
[3] R.Z. Rao, Science and technology of atmospheric effects on optical engineering: Progress in 3rd quinquennium of 21st century, Sci. China. Tech. Sci. 60 (2017) 1–13.
[4] J. Vernin, F. Roddier, Experimental determination of two-dimensional spatiotemporal power spectra of stellar light scintillation. Evidence for a multilayer structure of the air turbulence in the upper troposphere, J. Opt. Soc. Am. 63 (1973) 270–273.
[5] A.M. Schneidermant, D.P. Karo, Speckle interferometry measurements of atmospheric nonisoplanicity using double stars, J. Opt. Soc. Am. 68 (1978) 338–347.
[6] M. Sarazin, F. Roddier, The ESO differential Image motion monitor, Astron Astrophys. 227 (1990) 294–300.
[7] R.D. Marks, J. Vernin, M. Azouit, J.W. Briggs, M.G. Burton, M.C.B. Ashley, J.F. Manigault, Antarctic site testing-microthermal measurements of surface-layer seeing at the South Pole, Astron Astrophys. Suppl. Ser. 118 (1996) 385–390.
[8] R. Avila, J. Vernin, E. Masciadri, Whole atmospheric turbulence profiling with generalized scidar, Appl. Opt. 36 (1997) 7898–7905.
[9] V. Kornilov, A. Tokovinin, N. Shatsky, O. Voziakova, S. Potanin, B. Safonov, Combined mass-dimm instruments for atmospheric turbulence studies, Mon. Not. R. Astron. Soc. 382 (2007) 1268–1278.
[10] J.C. Wyngaard, On surface-layer turbulence, in Workshop on Micrometeorology, American Meteorological Society, Boston, Mass, 1973.
[11] K.L. Davidson, G.E. Schacher, C.W. Fairall, A.K. Goroch, Verification of the bulk method for calculating overwater optical turbulence, Appl. Opt. 20 (1981) 2919–2924.
[12] K.E. Kunkel, D.L. Walters, Modeling the diurnal dependence of the optical refractive index structure parameter, J. Geophys. Res. 88 (1983) 10999–11004.
[13] P.A. Frederickson, K.L. Davidson, C.R. Zeisse, C.S. Bendall, Estimating the refractive index structure parameters (C_n^2) over the ocean using bulk methods, J. Appl. Meteorol. 39 (2000) 1770–1783.
[14] S. Bendersky, N.S. Kopeika, N. Blaunstein, Atmospheric optical turbulence over land in middle east coastal environments: prediction modeling and measurements, Appl. Opt. 43 (2004) 4070–4079.
[15] D. Li, E. Bou-Zeid, H.A.R.D. Bruin, Monin-obukhov similarity functions for the structure parameters of temperature and humidity, Boundary-Layer Meteor. 145 (2012) 45–67.
[16] E. Masciadri, J. Vernin, P. Bougeault, 3D numerical simulations of optical turbulence at the roque de los muchachos observatory using the atmospherical model Meso-Nh, Astron. Astrophys. 365 (2001) 699–708.
[17] E. Masciadri, F. Lascaux, L. Fini, MOSE: operational forecast of the optical turbulence and atmospheric parameters at european southern observatory ground-based sites-I. overview and vertical stratification of atmospheric parameters at 0-20 km, Mon. Not. R. Astron. Soc. 436 (2013) 1968–1985.
[18] E. Masciadri, F. Lascaux, A. Turchi, L. Fini, Optical turbulence forecast: ready for an operational application, Mon. Not. R. Astron. Soc. 466 (2017) 520–539.
[19] F. Lascaux, E. Masciadri, S. Hagelin, Mesoscale optical turbulence simulations above Dome C, Dome A and South pole, Mon. Not. R. Astron. Soc. 411 (2011) 693–704.
[20] F. Lascaux, E. Masciadri, L. Fini, MOSE: operational forecast of the optical turbulence and atmospheric parameters at european southern observatory ground-based sites-II. atmospheric parameters in the surface layer 0-30 m, Mon. Not. R. Astron. Soc. 436 (2013) 3147–3166.

[21] F. Lascaux, E. Masciadri, L. Fini, Forecast of surface layer meteorological parameters at Cerro Paranal with a mesoscale atmospherical mode, Mon. Not. R. Astron. Soc. 449 (2015) 1664–1678.
[22] P. Pant, C.S. Stalin, R. Sagar, Microthermal measurements of surface layer seeing at devasthal site, Astron. Astrophys. Suppl. Ser. 136 (1999) 19–25.
[23] R.R. Beland, Infrared and electro-optical systems handbook, Environmental Research Institute of Michigan, SPIE Press, WA, 1993, pp. 161–176.
[24] X.Q. Wu, Q.G. Tian, P. Jiang, B. Chai, C. Qing, J. Cai, X.M. Jin, H.Y. Zhou, A new method of measuring optical turbulence of atmospheric surface layer at antarctic taishan station with ultrasonic anemometer, Adv. Polar. Sci. 26 (2015) 305–310.
[25] W.C. Skamarock, J.B. Klemp, J. Dudhia, Ncar technical note, NCAR/TN-475 + str Tech. rep. (2008).
[26] S.Y. Hong, J. Dudhia, S.H. Chen, A revised approach to ice microphysical processes for the bulk parameterization of clouds and precipitation, Mon. Weather Rev. 134 (2004) 2318–2341.
[27] E.J. Mlawer, S.J. Taubman, P.D. Brown, M.J. Iacono, S.A. Clough, Radiative transfer for inhomogeneous atmospheres: Rrtm, a validated correlated-k model for the longwave, J. Geophys. Res. 102 (1997) 16663–16682.
[28] M.D. Chou, M.J. Suarez, C.H. Ho, M.M.H. Yan, K.T. Lee, Parameterizations for cloud overlapping and shortwave single-scattering properties for use in general circulation and cloud ensemble models, J. Clim. 11 (1998) 202–214.
[29] Z.I. Janjic, The step-mountain eta coordinate model: Further developments of the convection, viscous sublayer, and turbulence closure schemes, Mon. Weather Rev. 122 (1994) 927–945.
[30] F. Chen, J. Dudhia, Coupling an advanced land surfacehydrology model with the penn state-ncar MM5 modeling system. part I: Model implementation and sensitivity, Mon. Weather Rev. 129 (2001) 569–585.
[31] M.B. Ek, K.E. Mitchell, Y. Lin, E. Rogers, P. Grunmann, V. Koren, G. Gayno, J.D. Tarpley, Implementation of noah land surface model advances in the national centers for environmental prediction operational mesoscale eta model, J. Geophys. Res. 108 (D22) (2003) 8851.
[32] G.L. Mellor, T. Yamada, Development of a turbulence closure model for geophysical fluid problems, Rev. Geophys. 20 (1982) 851–875.
[33] Z.I. Janjic, The step-mountain coordinate-physical package, Mon. Weather Rev. 118 (1990) 1429–1443.
[34] E.L. Andreas, Estimating C_n^2 over snow and ice from meteorological data, J. Opt. Soc. Am. A 5 (1988) 481–495.
[35] S. Pond, G.T. Phelps, J.E. Paquin, G. Mcbean, R.W. Stewart, Measurements of the Turbulent Fluxes of Momentum, Moisture and Sensible Heat over the Ocean, J. Atmos. Sci. 28 (1971) 901–917.
[36] C.A. Friehe, Estimation of the refractive-index temperature structure parameter over the ocean, Appl. Opt. 16 (1977) 334–340.
[37] P. He, S. Basu, Extending a surface-layer C_n^2 model for strongly stratified conditions utilizing a numerically generated turbulence dataset, Opt. Express. 24 (2016) 9574–9582.